World Academy of Science, Engineering and Technology
International Journal of Biomedical and Biological Engineering
Vol:7, No:9, 2013

Dynamic Ultrasound Scatterer Simulation Model Using Field-II and FEM for Speckle Tracking

Aws Al-azawi, John Soraghan

Open Science Index, Biomedical and Biological Engineering Vol:7, No:9, 2013 publications.waset.org/16850/pdf

***Abstract*—**There is a growing interest in the use of ultrasonic speckle tracking for biomedical image formation of tissue deformation. Speckle tracking is angle independent and has an ability to differentiate soft tissue into benign and malignant regions. In this paper a simulation model for dynamic ultrasound scatterer is presented. The model composes Field-II ultrasonic scatterers and FEM (ANSYS-11) nodes as a regional tissue deformation. A performance evaluation is presented on axial displacement and strain fields estimation of a uniformly elastic model, using speckle tracking based 1D cross-correlation of optimally segmented pre and post-deformation frames. Optimum correlation window length is investigated in terms of highest signal-to-noise ratio (SNR) for a selected region of interest of a smoothed displacement field. Finally, gradient based strain field of both smoothed and non-smoothed displacement fields are compared. Simulation results from the model are shown to compare favorably with FEM results.

***Keywords*—**Speckle tracking, tissue deformation, ultrasonic simulation.

I. Introduction

IN ultrasonic simulation, it is normal to use Field-II software to model different transducer and media scenarios [1], [2]. An alternative software suite is presented [3] however Field-II is regarded as more realistic, due to the fact that speckle is a multiplicative factor reflecting an interaction between sonography and media scatterers [4], [5]. These approaches deal with scatterers as static particles that are compatible for image analysis. For flow measurement, a dynamic scatterer isrequired, in which the above two approaches, may be developed in terms of scatterer motion and data acquisition in real time [6], [7].

Finite element modeling (FEM) has been used in simulations of complicated dynamic engineering problems [8]. As in speckle tracking, the speckle is repositioned according to the FEM model [9], the model is adequate for impulsive radiation force and is validated using phantom tissue experiments [9]. Further models have been developed for homogeneous and non-homogeneous nearly incompressible media under external compression using FEM, on linear array[10] and phase array [11] transducers using Field-II.

The objective of this work is in the construction of a framework of raw simulated data that represent backscatter from a tensile tissue under compression, using a combination of FEM and Field-II software.

Performance evaluation of the framework is conducted on displacement and strain field estimation in terms of optimization process to select best window length. The optimum window length has been selected to maximize the signal-to-noise ratio (SNR) of smooth displacement field, rather than the strain field [12], due to the highly error variance of the gradient operation [13]. The variance of the displacement field in the direction of applied compression is a function of the wavelength, physical characteristics of the object, and a compressing scenario, [14], [15]. In the case of partially coherent signals [16], a window length is a parameter that limits enough information of coherency between cross signals in terms of decorrelation noise.

The remainder of the paper is organized as follows. In section two a mathematical model of the composition process is presented, while section three provides a discussion of simulation results. In the last section conclusions and future work are presented.

II. Methodology

A proposed model of using Field-II software [1] for ultrasonic raw data acquisition to form pre-deformation (reference) and post-deformation (comparison) frames is designed. These frames represent raw-images data of homogeneous soft tissue before and after applied compression. In Fig. 1, a block diagram of proposed methodology is shown. The Field-II model uses a pre-deformation scatterer model to form the reference raw-data, and a post-deformation scatterer model to form comparison raw-data. The scatterer positions are moved in pre-deformation scatterer model according to the FEM (ANSYS-11) model to create the post-deformation scatterer model using our proposed scatterer-nodes composition algorithm. The composition algorithm is designed to associate each scatterer position in the Cartesian space coordinate with the closest four nodes of FEM model based on distance, and then moving it according to weighted displacement information of the FEM model. In the FEM model, the displacement information is created as a result of compression model (applied compression and degree of freedom). Finally, axial displacement field is estimated using speckle tracking technique of 1D cross-correlation for raw simulation data of pre- and post-deformation, while a gradient of displacement vector is used to form a strain field as illustrated in Fig. 1.

A. Al-azawi is with the Centre for Excellence in Signal and Image Processing, University of Strathclyde, Glasgow, Scotland, on study leave from the Mosul Technical College, Mosul, Iraq (Tel:+44 (0) 141 5482205; e-mail: aws.al-azawi@ strath.ac.uk).

J. Soraghan is with the Centre for Excellence in Signal and Image Processing, University of Strathclyde, Glasgow, Scotland (Tel: +44 (0) 141 5482514; e-mail: j.soraghan@ strath.ac.uk).

Open Science Index, Biomedical and Biological Engineering Vol:7, No:9, 2013 publications.waset.org/16850/pdf

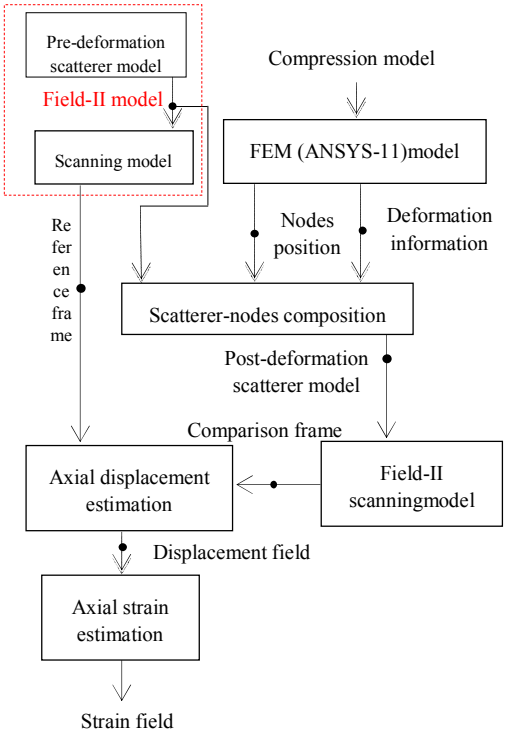


Fig. 1 Block diagram of proposed methodology

A. Field-II Model

A linear scan of a uniformly distributed 100000 scatterers in a cuboid dimension L x B x H mm where L=50mm is the length, B=10mm is the breadth, and H=50mm is the heights performed using a candidate Field-II package [17]. A linear array transducer is formed using a Hamming apodisation in-line aperture on transmit and receive imaging scenario of parameters using 5 MHz operating frequency, 50 MHz sampling frequency, 1540m/s constant speed of sound over the whole media, 0.31mm width of element, 5mm element height, 15.4µm kerf, 50mm focusing in axial direction, 1 sub-division in element length, 5 sub-divisions in element width, 128 and 64 total and active elements respectively.

A Hann envelope is selected as the transmitting pulse shape to smooth the low sidebands power spectrum [18], while the received signal is calculated as a backscatter reflections from a collection volume of scatterers using the Field-II function '*calc_scat'* command. The amplitudes are randomly Gaussian distributed over the whole scatterers and consequently the sonographic volume resolution of scatterers exhibits a Rayleigh amplitude distribution [19].

B. FEM Model

ANSYS-11 software is employed to form a homogeneous soft tissue that is linearly elastic. For this a Young's modulus of 20 kPa and Poisson's ratio of 0.495 is used [10] as an isotropic nearly incompressible material with a tetrahedral meshing of 35000 nodes located in the same cuboid dimension and space location of Field-II modelas given in Section II *A*.

Assume a compression is applied to the (L x B) surface of the homogeneous cuboid described in section II-A with the base constrained to move in the (x,y) plane only. This results in a displacement of H_d mm in the z direction and an ideal strain field of;

$$S = \frac{H_d}{H} \tag{1}$$

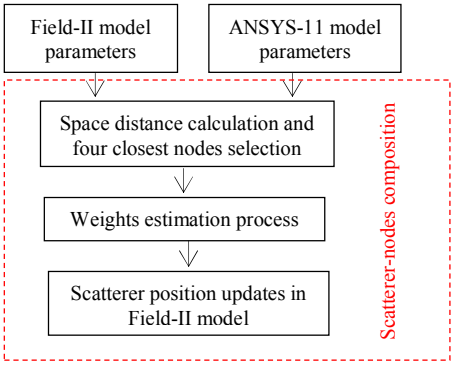


Fig. 2 Scatterer-nodes composition algorithm flowchart

C. Scatterer-Nodes Composition

The main input parameters of the composition algorithm are imported from Field-II and ANSYS-11 simulation models, as illustrated in Fig. 2. Field-II provides the scatterers' space location in the pre-deformation state of the 3D object (x_s^r, y_s^r, z_s^r), while ANSYS-11 exports the nodes space location $(x_{N_n}, y_{N_n}, z_{N_n})$ and displacement information $(disp_n^x, disp_n^y, disp_n^z)$, n = 1,2,3,4. The least distant four nodes from each scatterer are localized and defined as a displacement unit represented by tetrahedral structure as shown in Fig. 3, where N_n, S, and d_n, represents node, scatterer, and distance respectively.

In Fig. 3, the displacement information of the nodes are weighted and added to the scatterer space location S. As a consequence, all scatterers will be displaced to represent the 3D object of post-deformation state (x_s^c, y_s^c, z_s^c) in Field-II model, as follows:

$$x_s^c = x_s^r + \sum_{n=1}^{4} W_n^a \cdot disp_n^x \tag{2}$$

$$y_s^c = y_s^r + \sum_{n=1}^{4} W_n^a \cdot disp_n^y \tag{3}$$

$$z_s^c = z_s^r + \sum_{n=1}^{4} W_n^a \cdot disp_n^z \tag{4}$$

where

$$\sum_{n=1}^{n=4} W_n^a = 1 \tag{5}$$

and W_n^a is n-th weight.

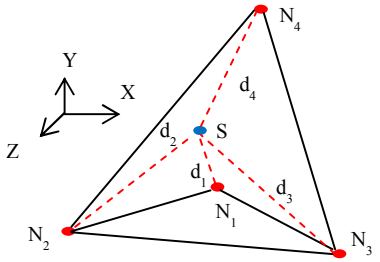


Fig. 3 Tetrahedral structure unit

In the scatterer nodes composition block shown in Fig. 2, an actual weight (W_n^a) of each node is estimated based on a distance ratio which is described as follows:

Firstly, in the Cartesian space, the distance d_n from each node $(x_{N_n}, y_{N_n}, z_{N_n})$ to a certain scatterer (x_s^r, y_s^r, z_s^r) is calculated as:

$$d_n = \sqrt{\left(x_s^r - x_{N_n}\right)^2 + \left(y_s^r - y_{N_n}\right)^2 + \left(z_s^r - z_{N_n}\right)^2} \quad (6)$$

The distances are sorted and four closest nodes are selected as input parameters to the weight estimation process as:

$$d_1 < d_2 < d_3 < d_4 \quad (7)$$

Secondly, an iterative estimation of the actual weights is performed. For this an initial distance state is assumed as

$$d_1^0 = d_2^0 = d_3^0 = d_4^0 \quad (8)$$

producing the following initial estimation of weights

$$W_n^0 = \left(\frac{1}{\text{no. of nodes}}\right) = 0.25, \quad n = 1, 2, 3, \text{and } 4 \quad (9)$$

In the first iteration, d_4 is considered as the most distant node.

$$d_1^0 = d_2^0 = d_3^0 < d_4 \quad (10)$$

and the actual weight of node four is computed using a distance ratio as

$$W_4^a = \frac{d_1}{d_4} . W_4^0 \quad (11)$$

The difference in weight of W_4^a and W_4^0 will be shared equally to the weights of other equidistant nodes (1, 2, and 3).

$$W_n^1 = W_n^0 + \left(\frac{W_4^0 - W_4^a}{3}\right) > W_n^0, \; n = 1, 2, \text{and } 3 \quad (12)$$

In the second iteration, d_3 is considered as the second furthest node from the scatterer

$$d_1^0 = d_2^0 < d_3 < d_4 \quad (13)$$

The actual weight of third node is estimated as:

$$W_3^a = \frac{d_1}{d_3} . W_3^1 \quad (14)$$

The difference in actual and iterative weights is divided equally and added to the weights of both first and second nodes as follows:

$$W_n^2 = W_n^1 + \left(\frac{W_3^1 - W_3^a}{2}\right) > W_n^1, \; n = 1 \text{ and } 2 \quad (15)$$

In the third iteration step, d_2 is considered as the third furthest node from the scatterer

$$d_1^0 < d_2 < d_3 < d_4 \quad (16)$$

and the actual weights of both first and second nodes are

$$W_2^a = \frac{d_1}{d_2} . W_2^2 \quad (17)$$

$$W_1^a = W_1^2 + (W_2^2 - W_2^a) \quad (18)$$

By combining (11), (14), (17) and (18) it can be shown that the summation of actual weights is unity as required from (5).

C. Axial Displacement / Strain Field Estimation

A block diagram of the axial displacement and strain filed estimation algorithm is shown in Fig. 4. The deformation of the object under compression is obtained by estimation of displacement and strain in the direction of applied compression. Each raw-line in the frame is segmented based on an optimum window that is considered for a range of lengths as a function of signal-to-noise ratio for a region of interest within the smoothed displacement field. The speckle tracking approach uses normalized 1-D cross-correlation between equally segmented pre- and post-deformation windows. A continuous displacement field *D* is assumed and low lateral decorrelation noise is expected due to a small axial displacement of 0.1mm that is applied. A spline interpolation is employed for subsample displacement estimation of the correlation peak locations [11]. Sequential windows are overlapped by 50% to form less noisy strain estimates [20].

An algorithm refinement is employed that smooth out fluctuations in the axial displacement field, using a moving average window as a pre-processing step toward noise reduction in strain estimation.

Finally, the strain field is estimated using the classical gradient of the displacement vector [20] as:

$$S = (D_{i+1} - D_i)/L_o \quad (19)$$

Open Science Index, Biomedical and Biological Engineering Vol:7, No:9, 2013 publications.waset.org/16850/pdf

Open Science Index, Biomedical and Biological Engineering Vol:7, No:9, 2013 publications.waset.org/16850/pdf

where D_i and D_{i+1} are displacement components of depth i and $i+1$ respectively,L_o is a length of window overlap.

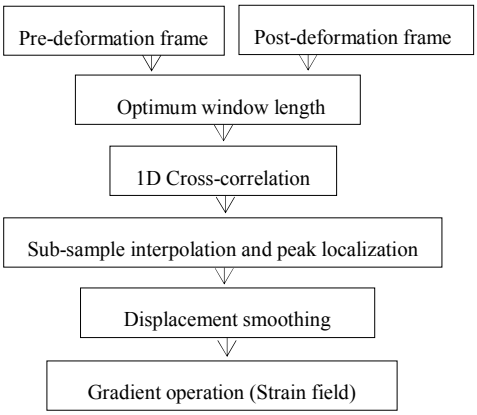


Fig. 4 Axial displacement and strain estimation diagram

III. Results and Discussion

As described in section II-B, axial compression of 0.1mm is applied to one face of a cuboid object. Using the simulation parameters described in Section II, pre-deformation and post-deformation frames were used to produce a non-interpolated axial displacement field using the algorithm described in section II-D as shown in Fig. 5 (a). Note: In Fig. 5, all color bars represent the displacement in meters. The ideal field obtained from FEM is shown in Fig. 5 (b). In this the displacement field is consistent. Fig. 5 (a) shows a max displacement of 0.092e-3 m, while in Fig. 5 (b) it is measured as 0.1e-3 m resulting in an error in displacement estimation of 8µm. This error of 8% is an accounted by a combination of algorithmic error, randomness of scatterer locations, and meshing structure of FEM object.

A Spline interpolation is used for subsample peak location of 1D cross-correlation to form Fig. 5 (c). The image is smoothed in the axial direction using a 16-length moving average to form Fig. 5 (d).

Optimization for the best correlation window length is presented in Table I for range of lengths (1 – 6λ) in steps of 0.5λ as a function of SNR_{dB} of smoothed displacement field for a selected region of interest that is highlighted in the dashed rectangular box shown in Fig. 5 (d). The table indicates a positive relation between window length and SNR_{dB}. This is in agreement with the assumption of involving more information of cross signals coherency[15],even though some fluctuations related to a small effects of the decorrelation noise. A dip in SNR_{dB} of 23.20is pointed as optimum window length that provides good axial resolution of 3.5λ.

From (1) the ideal strain field of FEM is a uniform of 0.2%. The strain field is obtained from (19) without displacement smoothing is shown in Fig. 6 (a), in which a variance in estimation is related to the high fluctuations in displacement. While, the strain field with displacement smoothing is shown in Fig. 6 (b). In which the variance is reduced, to be nearly uniform and consistent in ideal of 0.2%.

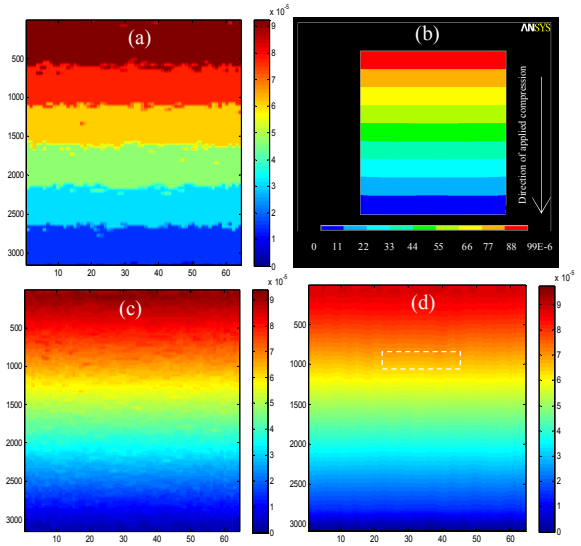


Fig. 5 Non-interpolated (a), FEM (b), interpolated (c), and smoothed (d) displacement field

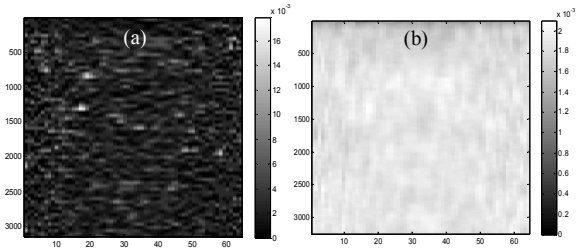


Fig. 6 Stain field without (a), and with (b) displacement smoothing

IV. Conclusion and Future Work

A data set comprising a simulation framework designed by composition of ultrasonic simulation software (Field-II) and a finite element model (ANSYS-11) has been presented. The scatterers are translated in Cartesian coordinate according to displacement vectors of ANSYS-11. Cross-correlation is exploited as a speckle tracking, by using a development in terms of displacement field smoothing and coherent window length optimization. Results reflect a good agreement with the ideal state of ANSYS-11 model. Further development on strain estimation process will investigate the reduction of the dynamic range of strain variance. Non-homogeneous object of hard inclusion is in development as complex state of algorithm evaluation. Experimentally, an in-vitro validation is targeted using a tissue mimicking material and ultrasonic system that provides a raw data of acquisition.

TABLE I
OPTIMALWINDOW LENGHT

Window length (λ)	1	1.5	2	2.5	3	**3.5**	4	4.5	5	5.5	6
SNR (dB)	17.69	15.55	20.88	20.05	20.63	**23.20**	21.44	20.90	22.04	22.19	22.13

ACKNOWLEDGMENT

The authors are grateful to the ministry of higher education and scientific research of Iraq for funding support and also to Jerzy Dziewierz for beneficial discussion.

REFERENCES

[1] http://field-ii.dk/?background.html.
[2] Jensen, J.A. and N.B. Svendsen, Calculation of pressure fields from arbitrarily shaped, apodized, and excited ultrasound transducers. Ultrasonics, Ferroelectrics and Frequency Control, IEEE Transactions on, 1992. 39(2): p. 262-267.
[3] Meunier, J. and M. Bertrand, Ultrasonic texture motion analysis: theory and simulation. Medical Imaging, IEEE Transactions on, 1995. 14(2): p. 293-300.
[4] Thijssen, J.M. and B.J. Oosterveld. Speckle and Texture in Echography: Artifact or Information? in IEEE 1986 Ultrasonics Symposium. 1986.
[5] Wagner, R.F., M.F. Insana, and S.W. Smith, Fundamental correlation lengths of coherent speckle in medical ultrasonic images. Ultrasonics, Ferroelectrics and Frequency Control, IEEE Transactions on, 1988. 35(1): p. 34-44.
[6] Jensen, J.A. Simulation of advanced ultrasound systems using Field II. in Biomedical Imaging: Nano to Macro, 2004. IEEE International Symposium on. 2004.
[7] Marion, A. and D. Vray, Toward a real-time simulation of ultrasound image sequences based on a 3-D set of moving scatterers. Ultrasonics, Ferroelectrics and Frequency Control, IEEE Transactions on, 2009. 56(10): p. 2167-2179.
[8] Madenci, E. and I. Guven, The Finite Element Method And Applications In Engineering Using ANSYS. Springer, 2006.
[9] Palmeri, M.L., et al., A finite-element method model of soft tissue response to impulsive acoustic radiation force. Ultrasonics, Ferroelectrics and Frequency Control, IEEE Transactions on, 2005. 52(10): p. 1699-1712.
[10] Lopata, R.G.P., et al., Performance Evaluation of Methods for Two-Dimensional Displacement and Strain Estimation Using Ultrasound Radio Frequency Data. Ultrasound in Medicine & Biology, 2009. 35(5): p. 796-812.
[11] Lopata, R.G.P., 2D and 3D Ultrasound Strain Imaging: Methods and in vivo Applications. PhD Thesis, Radboud University Nijmegen, 2010.
[12] Varghese, T., M. Bilgen, and J. Ophir, Multiresolution imaging in elastography. Ultrasonics, Ferroelectrics and Frequency Control, IEEE Transactions on, 1998. 45(1): p. 65-75.
[13] Kallel, F. and J. Ophir, A least-squares strain estimator for elastography. Ultrason Imaging, 1997. 19: p. 195–208.
[14] Bilgen, M. and M.F. Insana, Error analysis in acoustic elastography. I. Displacement estimation estimation. Acoustical Society of America, 1997. 101(2).
[15] Ophir, J., et al., Elastography: Ultrasonic estimation and imaging of the elastic properties of tissues. Proceedings of the Institution of Mechanical Engineers, Part H: Journal of Engineering in Medicine, 1999. 213(3): p. 203-233.
[16] Walker, W.F. and G.E. Trahey, A fundamental limit on delay estimation using partially correlated speckle signals. Ultrasonics, Ferroelectrics and Frequency Control, IEEE Transactions on, 1995. 42(2): p. 301-308.
[17] Jensen, J.a., Field: a Program For simulating Ultrasound systems. Med. Biol. Eng. Comput, 1996. 34(1 , Part 1): p. 1351-1353.
[18] Hoff, L., Acoustic Characterization of Contrast Agents for Medical Ultrasound Imaging. Kluwer Academic Publishers, 2001.
[19] Wagner, R.F., et al., Statistics of Speckle in Ultrasound B-Scans. Sonics and Ultrasonics, IEEE Transactions on, 1983. 30(3): p. 156-163.
[20] Bilgen, M. and M.F. Insana, Error analysis in acoustic elastography. II. Strain estimation and SNR analysis. Acoustical Society of America, 1997. 101(2): p. 1147-1154.

Open Science Index, Biomedical and Biological Engineering Vol:7, No:9, 2013 publications.waset.org/16850/pdf